A SUPERCONVERGENT ALGORITHM FOR INVARIANT SPIN FIELD STROBOSCOPIC CALCULATIONS*

David Sagan, Cornell University, Ithaca, NY, 14850, USA

Abstract

Stroboscopic averaging can be used to calculate the invariant spin field $\mathbf{n}$ for particles with a finite oscillation amplitude in phase space. The standard technique starts with making a guess for $\mathbf{n}(\mathbf{r})$, which is a function of the phase space position $\mathbf{r}$. By tracking a particle's orbital position forward in time and then projecting the guessed $\mathbf{n}$ backwards to the starting phase space point, the average of the backward projected spins will converge to the invariant spin field direction linearly as $1/N$ where N is the number of turns tracked. The convergence can be accelerated by an iterative method that uses an approximate invariant spin field constructed by averaging the calculated spin field over points that are close in orbital phase space. This superconvergent algorithm has been built into a new program based upon the Bmad toolkit for charged particle and X-ray simulations.

INTRODUCTION

In a storage ring, the invariant spin field $\mathbf{n}(\mathbf{r}, s)$, which is a function of the 6-dimensional phase space position $\mathbf{r}$ and the longitudinal position s, is the solution, with unit normalization, to the Thomas-Bargmann-Michel-Telegdi (T-BMT) equation such that [1]

$$\mathbf{R}(\mathbf{r}, s)\,\mathbf{n}(\mathbf{r}, s) = \mathbf{n}(\mathbf{M}\,\mathbf{r}, s)\,, \qquad (1)$$

where $\mathbf{M}$ is the one-turn orbital map, and $\mathbf{R}$ is the one-turn spin map. The concept of the invariant spin field, which was first introduced by Derbenev and Kondratenko [2], is important since it can be used to calculate the maximum achievable time averaged polarization [3] as well as the spin depolarization rate due to synchrotron radiation [4].

There are several methods that can be used to calculate the invariant spin field. Adiabatic anti-damping [5], the SODOM-2 algorithm [6], normal form analysis of the spin/orbital transfer map [7] and stroboscopic averaging [3] are the major methods. The method considered in this paper is stroboscopic averaging. There are several similar variants for stroboscopic averaging [1]. The most efficient of these variants starts with a particle at some given longitudinal position s and some phase space position $\mathbf{r} = (\mathbf{J}_0, \boldsymbol{\Phi}_0)$ where $(\mathbf{J}_0, \boldsymbol{\Phi}_0)$ are the particle's coordinates expressed using action-angle variables. The particle is tracked N turns. The invariant spin field at the starting position is then approximated by

$$\mathbf{n}(\boldsymbol{\Phi}_0) \simeq \frac{\mathbf{n}_{\text{ave}}}{|\mathbf{n}_{\text{ave}}|}, \quad \mathbf{n}_{\text{ave}} = \frac{1}{1+N} \sum_{i=0}^{N} \mathbf{R}^{-1}(\boldsymbol{\Phi}_0, \boldsymbol{\Phi}_i)\, \widetilde{\mathbf{n}}(\boldsymbol{\Phi}_i),$$

$$(2)$$

where $\mathbf{R}(\boldsymbol{\Phi}_0, \boldsymbol{\Phi}_i)$ is the spin rotation matrix from orbital phase $\boldsymbol{\Phi}_0$ to $\boldsymbol{\Phi}_i$, and $\widetilde{\mathbf{n}}(\boldsymbol{\Phi}_n)$ is a guessed value for the $bfn(\boldsymbol{\Phi}_n)$ on the nth turn at orbital phase $\boldsymbol{\Phi}_n$. Here and below, the dependence on $\mathbf{J}$ (which is a constant of the motion) and s has been suppressed. The guessed value is typically taken to be the value of the closed orbit invariant spin field direction $\mathbf{n}_0$. The average of the backward projected spins will converge to the true $\mathbf{n}(\boldsymbol{\Phi}_0)$ as the number of turns tracked increases to infinity. Once $\mathbf{n}(\boldsymbol{\Phi}_0)$ has been calculated, bfn can be calculated at other points by forward propagation

$$\mathbf{n}(\boldsymbol{\Phi}_i) = \mathbf{R}(\boldsymbol{\Phi}_0, \boldsymbol{\Phi}_i)\, \mathbf{n}(\boldsymbol{\Phi}_0)\,. \qquad (3)$$

The convergence of this algorithm is linear with $1/N$ [1]. Neglected in this algorithm is the fact that, since $\mathbf{n}$ is a continuous function, if $\boldsymbol{\Phi}_i$ is close to $\boldsymbol{\Phi}_j$, then $\mathbf{n}(\boldsymbol{\Phi}_i)$ must be close to $\mathbf{n}(\boldsymbol{\Phi}_j)$. By changing the algorithm to minimize the scatter in $\mathbf{n}$ at points that are close to each other in orbital space, an accelerated convergence can be achieved. This is discussed below. The convergence speed is potentially important, for example, in lattice design where many lattice configurations may need to be considered.

SUPERCONVERGENT ALGORITHM

The new stroboscopic algorithm has two variants which will be called the "self-consistent" variant and the "scatter-minimization" variant. The common feature of the two variants involves tracking a particle beginning at some given phase space point over some number N of turns. After each turn, the phase space position and the 1-turn spin transfer matrix are stored. Since the spin transfer matrix only has a few components, the amount of storage needed is negligible even over many turns. With respect to computation time, matrix multiplication of 1-turn spin matrices is very fast compared to the time it takes to track a particle in a realistic lattice. Therefore, the simulation time is essentially proportional to N and is independent of the algorithm, old or new, used to calculate $\mathbf{n}$. With any algorithm, convergence to the true value of $\mathbf{n}$ can be tested by calculating $\mathbf{n}$ periodically as the particle is tracked and then stopping when changes in the value of $\mathbf{n}$ fall below a given tolerance.

The new algorithm relies on the fact that, away from any spin-orbit resonances (and it is assumed in this paper that the system is not on a spin-orbit resonance), $\mathbf{n}(\mathbf{r})$ is a smooth continuous function of $\mathbf{r}$. This means that $\mathbf{n}$ at a given phase space point can be approximated by an average of the values for $\mathbf{n}$ computed at nearby points in orbital phase space.

Self-Consistent Algorithm Variant

The self-consistent algorithm is based on the fact that if the guessed $\widetilde{\mathbf{n}}(\boldsymbol{\Phi}_i)$ in Eq. (2) are in the same direction as the

actual $\mathbf{n}(\boldsymbol{\Phi}_i)$, then the calculated $\mathbf{n}(\boldsymbol{\Phi}_0)$ will be exact. The aim of the algorithm is to use a more accurate $\widetilde{\mathbf{n}}(\boldsymbol{\Phi}_i)$ in place of what is used in the standard algorithm.

With the self-consistent algorithm, initially, after N turns of tracking, $\mathbf{n}(\boldsymbol{\Phi}_0)$ is calculated using the old "standard" calculation. After this, the self-consistent algorithm uses the following loop:

1. Compute $\mathbf{n}(\boldsymbol{\Phi}_i)$ for all $i = 1, \ldots, N$ by applying Eq. (3).

2. For all $i = 0, \ldots, N$, average the $\mathbf{n}$ that are near $\mathbf{n}(\boldsymbol{\Phi}_i)$ to produce a new guess $\widetilde{\mathbf{n}}(\boldsymbol{\Phi}_i)$.

3. Use $\widetilde{\mathbf{n}}(\boldsymbol{\Phi}_i)$ in Eq. (2) to calculate a new $\mathbf{n}(\boldsymbol{\Phi}_0)$.

4. If the new $\mathbf{n}(\boldsymbol{\Phi}_0)$ is within a user defined tolerance of the old $\mathbf{n}(\boldsymbol{\Phi}_0)$, stop. If not, go back to step 1 and keep looping until convergence is achieved.

There are various algorithms that could be used to calculate the averaged $\widetilde{\mathbf{n}}$. The one chosen in the simulations below involves averaging over the "directional nearest neighbors". There are six directional nearest neighbors, one for each of the directions $\pm\Phi_x$, $\pm\Phi_y$ and $\pm\Phi_z$. For example, the $+\Phi_y$ nearest neighbor to the point $\boldsymbol{\Phi}_i$ is the nearest neighbor point $\boldsymbol{\Phi}_j$ such that $d\Phi_{ji,y} \equiv \Phi_{j,y} - \Phi_{i,y}$ is positive or zero with $|d\Phi_{ji,x}| \leq |d\Phi_{ji,y}|$ and $|d\Phi_{ji,z}| \leq |d\Phi_{ji,y}|$. [Care must be taken here to evaluate $d\Phi_{ji}$ components modulo factors of 2π.] The other directional nearest neighbors are calculated similarly. The weighted average is then

$$\widetilde{\mathbf{n}}(\boldsymbol{\Phi}_i) = \sum_{j \in \gamma(i)} \frac{\mathbf{n}(\boldsymbol{\Phi}_j)}{\max(\alpha, |d\boldsymbol{\Phi}_{ji}|)}, \qquad (4)$$

where $\gamma(i)$ is the set of six indicies for the nearest neighbor points and α is a tiny positive constant used to prevent divide by zero problems. The $\max(\alpha, |d\boldsymbol{\Phi}_{ji}|)$ denominator is a weighting factor so that points that are close to $\boldsymbol{\Phi}_i$ are weighted more.

Notice that the magnitude of $\widetilde{\mathbf{n}}(\boldsymbol{\Phi}_i)$ is not normalized to one so that points that have nearest neighbors that are close by (that is small $|d\boldsymbol{\Phi}_{ji}|$) contribute more to the sum in Eq. (2). Since the calculation of $\widetilde{\mathbf{n}}(\boldsymbol{\Phi}_i)$ will be more accurate when the nearest neighbor points are closer, the convergence of the algorithm is helped by effectively using a higher weight for such points. In fact, in the case where a nearest neighbor point has $\boldsymbol{\Phi}_j$ equal to $\boldsymbol{\Phi}_i$, the self-consistent algorithm will converge to the exact solution in the limit that α is vanishingly small.

Scatter-Minimization Algorithm Variant

The scatter-minimization algorithm is based upon the fact that in some sense the difference ("scatter") between $\mathbf{n}(\boldsymbol{\Phi}_i)$ and the averaged value of the nearest neighbor points should be small since $\mathbf{n}$ is a continuous function. Thus the scatter-minimization algorithm involves varying the direction of $\mathbf{n}(\boldsymbol{\Phi}_0)$ to minimize a merit function M that is a measure of

the scatter:

$$M = \sum_{i=0}^{N} \left[\sum_{j \in \gamma(i)} \frac{\mathbf{n}(\boldsymbol{\Phi}_j) - \mathbf{n}(\boldsymbol{\Phi}_i)}{\max(\alpha, |d\boldsymbol{\Phi}_{ji}|)} \right]^2 . \qquad (5)$$

Like the self-consistent variant, terms in the merit function are weighted in favor of points where the nearest neighbor points are closest and, like the self-consistent variant, the scatter minimization variant will converge to the exact solution, in the limit that α is vanishingly small, if two track points coincide in orbital space.

SIMULATIONS

The self-consistent and scatter-minimization algorithms, along with the standard stroboscopic averaging technique have been built into a new simulation program called "Spin_Stroboscope". This program uses the Bmad toolkit for charged particle and X-ray simulations [8] as a basis for tracking.

To benchmark the algorithms, simulations were done using a model which is an extension of the standard one-resonance model [1]:

$$\frac{d\mathbf{s}}{d\theta} = \boldsymbol{\Omega}(\boldsymbol{\Phi}) \times \mathbf{s}, \qquad \frac{d\boldsymbol{\Phi}}{d\theta} = (Q_x, Q_y, Q_z) \qquad (6)$$

$$\boldsymbol{\Omega} = \begin{pmatrix} \epsilon_x \cos(\Phi_x) + \epsilon_y \cos(\Phi_y) + \epsilon_z \cos(\Phi_z) \\ \epsilon_x \sin(\Phi_x) + \epsilon_y \sin(\Phi_y) + \epsilon_z \sin(\Phi_z) \\ \nu_0 \end{pmatrix},$$

where ϵ_x, ϵ_y and ϵ_z are resonance strengths for the three modes, Φ_x, Φ_y, and Φ_z are the mode phases, ν_0 is the closed orbit spin tune, and θ is the longitudinal coordinate of the ring with a change in θ of 2π for one revolution of the beam. The orbital transport was linear with a constant phase advance (Q_x, Q_y, Q_z) per turn.
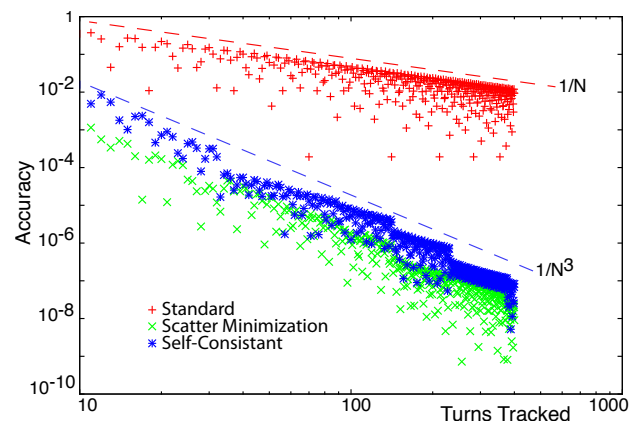

Figure 1: Simulation accuracy verses number of turns using a one-resonance model for the spin transport. Red: Standard stroboscopic averaging. Green: scatter-minimization calculation. Blue: self-consistent variant. The upper dashed line illustrates the slope for a $1/N$ convergence rate while the lower dashed line illustrates a $1/N^3$ convergence rate.
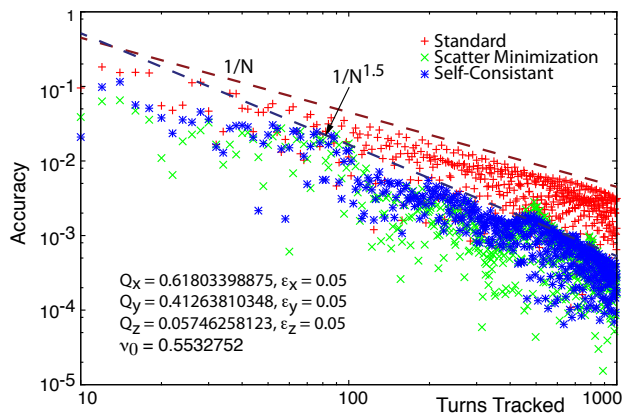
01 Circular and Linear Colliders

A24 Accelerators and Storage Rings, Other

Figure 2: Simulation accuracy verses number of turns using a three-resonance model for the spin transport and non-comensurate orbital tunes. Red: Standard stroboscopic averaging. Green: scatter-minimization calculation. Blue: self-consistent variant. The two dashed lines show convergence rates of $1/N$ and $1/N^{1.5}$.

Figure 3: Simulation Accuracy verses number of turns using a three-resonance model for the spin transport and commensurate orbital tunes. Red: Standard stroboscopic averaging. Green: scatter-minimization calculation. Blue: self-consistent variant.

The first simulation used a single excited mode to mimic a single resonance situation. The results are shown in Fig. 1 which shows the simulation accuracy, that is, the difference between the calculated and actual $\mathbf{n}(\Phi_0)$, as a function of the number of turns tracked for all three algorithms. Simulation parameters where $Q_x = (\sqrt{5}-1)/2$, $\nu_0 = 0.55$ and $\epsilon_x = 0.2$ with all other parameters set to zero. Q_x was chosen to be the fractional part of the golden ratio to be a "worst case" scenario for the two new algorithms since the golden ratio is the most irrational number possible and thus this case avoids having points in orbital phase space overlapping or being very close (that is, being much less than $1/N$).

Fig. 1 shows that the standard algorithm converges as $1/N$ as expected. The new algorithms converge much faster as $1/N^3$ with the scatter-minimization being a little bit better than the self-consistent calculation. An estimate of the convergence for the self-consistent calculation is as follows: The characteristic distance between nearest neighbor points $|d\Phi_{ji}|$ is $1/N$. Since Q_x is very irrational, it is expected that the denominators in Eq. (4) are similar and will be ignored. The difference between $\mathbf{n}(\Phi_j)$ in the numerator in Eq. (4) and $\mathbf{n}(\Phi_i)$ will scale as $|d\Phi_{ji}|$. That is, will scale as $1/N$. Since the sum in Eq. (4) is over nearest neighbor points (2 in this case) which are on opposite sides of Φ_i, it is expected that the first order difference will cancel out leaving a second order difference which scales as $|d\Phi_{ji}|^2$ or $1/N^2$. This error, when summed in Eq. (2), will be reduced by a factor of $1/N$ (just like in the standard algorithm). So the final error is $1/N^3$.

Results, with three modes excited, and using incommensurate tunes, is shown in Fig. 2. Values for the model parameters are also shown in the figure. Here the convergence of the standard algorithm is still $1/N$ as expected, and the convergence of the two variants is about $1/N^{1.5}$ at least above $N = 50$ or so. Extending the estimate calculation used in the
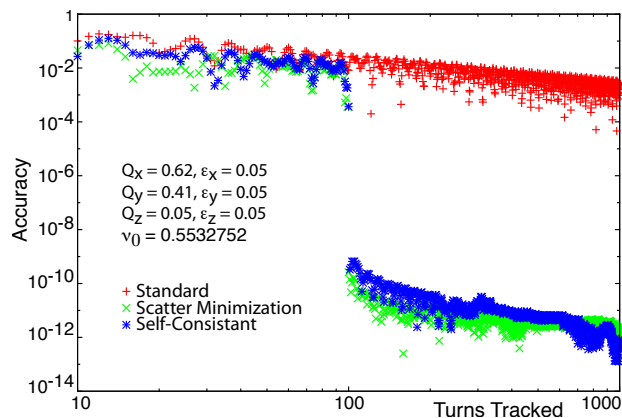
one-resonance model case to three dimensions gives a characteristic distance between nearest neighbor points $|d\Phi_{ji}|$ which scales as $1/N^{1/3}$. This gives an error in the calculated $\widetilde{\mathbf{n}}(\Phi_i)$ in Eq. (4) that scales as $1/N^{2/3}$ so that the error in calculating $\widetilde{\mathbf{n}}(\Phi_0)$ which is a factor of $1/N$ less is $1/N^{5/3}$ or $1/N^{1.67}$. Considering the crudeness of the estimate calculation, the simulated and estimated convergence rates should be considered to be in reasonable agreement with each other.

If the orbital tunes are made commensurate, both variants of the new algorithm will essentially converge on the exact result within a set number of turns. This is shown in Fig. 3 where the orbital tunes are commensurate every 100 turns. The reason why the error does not go to zero in this case is due to the finite value of α in Eqs. (4) and (5) which was set to 10^{-10} in this case. Of course since the tunes are commensurate this implies an orbital resonance. However, since the resonance is of order 100, in most situations, this will not be a problem.

CONCLUSION

A new stroboscopic averaging algorithm for the calculation of the invariant spin field has been presented. There are two variants of this algorithm with both variants showing similar convergence characteristics and both variants showing better convergence compared to the standard algorithm. In fact, if the orbital tunes can be made commensurate with each other, the new algorithm will essentially converge to the exact result in a set number of turns tracked.

Shorter computation times not only make existing simulations more efficient, but open the door for simulations that would not be practical before.

ACKNOWLEDGMENTS

REFERENCES

[1] G. Hoffstaetter, *High Energy Polarized Proton Beams: A Modern View*, ser. Springer Tracts in Modern Physics, , Vol. **218**. Springer New York, 2006, ISBN: 9780387347547.

[2] Y. S. Derbenev and A. M. Kondratenko, "Polarization kinetics of particles in storage rings," *Soviet Journal of Experimental and Theoretical Physics*, vol. 37, p. 968, Dec. 1973.

[3] K. Heinemann and G. H. Hoffstätter, "Tracking algorithm for the stable spin polarization field in storage rings using stroboscopic averaging," *Phys. Rev. E*, vol. 54, pp. 4240–4255, 4 Oct. 1996. DOI: 10.1103/PhysRevE.54.4240. https://link.aps.org/doi/10.1103/PhysRevE.54.4240

[4] A. W. Chao and M. Tigner, Eds., *Handbook Of Accelerator Physics And Engineering (3rd Printing)*. World Scientific Publishing Company, 2006, ISBN: 9789814496049.

[5] G. H. Hoffstaetter, M. Vogt, and D. P. Barber, "Higher-order effects in polarized proton dynamics," *Phys. Rev. ST Accel. Beams*, vol. 2, p. 114001, 11 Nov. 1999. DOI: 10.1103/PhysRevSTAB.2.114001. https://link.aps.org/doi/10.1103/PhysRevSTAB.2.114001

[6] K. Yokoya, "An Algorithm for calculating the spin tune in circular accelerators," 1999. arXiv: physics/9902068 [physics].

[7] E. Forest, *From Tracking Code to Analysis: Generalised Courant-Snyder Theory for Any Accelerator Model*. Springer Japan, 2016, ISBN: 9784431558033.

[8] D. Sagan, "Bmad: A relativistic charged particle simulation library," *Nuc. Instrum. & Methods Phys. Res. A*, vol. 558, pp. 356–59, 2006.